Suppression of TRPM7 by carvacrol protects against injured spinal cord by inhibiting blood-spinal cord barrier disruption

Chan Sol Park
Kyung Hee University
Jee Youn Lee
Kyung Hee University
Hae Young Choi
Kyung Hee University
Bong Gun Ju
Sogang University
Tae Young Yune (tyune@khu.ac.kr)
Kyung Hee University https://orcid.org/0000-0001-5242-5746

Research Article

Keywords: Transient receptor potential melastatin 7, TRPM7, blood-spinal cord barrier, spinal cord injury, Carvacrol

Posted Date: April 22nd, 2021

DOI: https://doi.org/10.21203/rs.3.rs-416918/v1

Version of Record: A version of this preprint was published at Journal of Neurotrauma on February 16th, 2022. See the published version at https://doi.org/10.1089/neu.2021.0338.

Abstract

When the blood-spinal cord barrier (BSCB) is disrupted after a spinal cord injury (SCI), several pathophysiological cascades occur, including inflammation and apoptotic cell death of neurons and oligodendrocytes, resulting in permanent neurological deficits. Transient receptor potential melastatin 7 (TRPM7) is involved in the pathological processes in many neuronal diseases, including traumatic brain injury, amyotrophic lateral sclerosis, parkinsonism dementia, and Alzheimer's disease. Furthermore, carvacrol (CAR), a TRPM7 inhibitor, is known to protect against SCI by reducing oxidative stress and inhibiting the endothelial nitric oxide synthase pathway. However, the functions of TRPM7 in the regulation of BSCB homeostasis after SCI have not been examined. Here, we demonstrated that TRPM7, a calcium-mediated non-selective divalent cation channel, plays a critical role after SCI in rat. Rats were contused at T9 and given CAR (50 mg/kg) via intraperitoneally immediately and 12 hours after SCI, and then given the same dose once a day for 7 days. TRPM7 was found to be up-regulated after SCI in both in vitro and in vivo studies, and it was expressed in blood vessels alongside neurons and oligodendrocytes. Additionally, CAR treatment suppressed BSCB disruption by inhibiting the loss of TJ proteins and preserved TJ integrity. CAR also reduced apoptotic cell death and improved functional recovery after SCI by preventing BSCB disruption caused by blood infiltration and inflammatory responses. Based on these findings, we propose that blocking the TRPM7 channel can inhibit the destruction of the BSCB and it is a potential target in therapeutic drug development for use in SCI.

Introduction

Spinal cord injury (SCI) is a devastating condition that results in permanent disability and thereby influences a profound effect on the quality of life. It causes dysfunction of the limbs and trunk below the injured region and leads to spinal cord edema, apoptotic cell death and permanent disability [1]. Despite years of intensive research, there are no widely accepted therapies to reduce tissue injury and enhance functional recovery after SCI. Initial mechanical damage causes necrosis and blood vessel rupture at the site of the lesion. After that, a series of pathological events occur in response to the primary injury, resulting in a secondary injury that affects both the wound and the surrounding area. Especially, hemorrhage, impaired blood flow, and blood-spinal cord barrier (BSCB) disruption are critical events that cause secondary damage, which results in chronic permanent dysfunction after SCI [1]. When the BSCB is disrupted, blood cells like neutrophils and macrophages infiltrate the spinal tissue and produce inflammatory mediators like pro-inflammatory cytokines, which contribute to secondary injuries [2, 3]. Therefore, the development of therapeutic agents inhibiting BSCB disruption would be useful for the restriction of secondary injury followed functional recovery after SCI.

Extensive ion imbalances, including calcium overload in the spinal cord after a traumatic injury, causes irreversible damage to various cellular functions such as protein synthesis, and mitochondria, cytoskeleton, and cell membrane functions, which is one of the leading causes of cell death [4]. Transient receptor potential (TRP) ion channels, which are non-selective cation channels, are expressed in many cells and tissues, including neurons and endothelial cells of the nervous system and have been shown to

play important roles in diverse cellular processes [5, 6]. The TRP melastatin 7 (TRPM7) channel, in particular, is a metal ion-permeable, non-selective cation channel that is expressed in almost all tissues [7] and regulates divalent cation (Mg^{2+}, Ca^{2+}, and Zn^{2+}) homeostasis [8, 9], cell survival, proliferation, cell adhesion, and Ca^{2+}-mediated neurotransmitter release [10].

TRPM7 has been shown to play an important role under pathological conditions [11], although its function has been mainly researched in neurons. Previous studies indicated that TRPM7 mediates the death of anoxic neurons by regulating Ca^{2+} influx during cerebral ischemia and prolonged oxygen-glucose deprivation [12–14]. The suppression of TRPM7 after brain ischemia also facilitated neuron survival and preserved the morphology and function of neurons in hippocampal CA1 [15]. Additionally, it was reported that TRPM7 is involved in the pathologic processes of some neurodegenerative diseases including western pacific amyotrophic lateral sclerosis, parkinsonism dementia, and Alzheimer's disease [16, 17]. Furthermore, carvacrol (CAR), a TRPM7 inhibitor, is known to protect against SCI by suppressing oxidative damage and the endothelial nitric oxide synthase pathway [18]. However, the functions of TRPM7 in the regulation of BSCB homeostasis after SCI have not been examined.

In the present study, we examined the role of TRPM7 by investigating the effect of CAR on BSCB disruption after SCI in rats. Our study showed that the expression of TRPM7 was up-regulated after SCI, and its expression was observed in blood vessels including neurons and oligodendrocytes. Additionally, treatment with CAR, a TRPM7 inhibitor, reduced apoptotic cell death and improved functional recovery by preventing BSCB disruption followed blood infiltration and inflammatory responses after SCI.

Materials And Methods

Animal model of SCI

Adult male Sprague-Dawley rats (250–300 g, Samtako, Osan, Korea) were used in this study. Before surgery, rats were weighed and anesthetized with 500 mg/kg of chloral hydrate (i.p.). Laminectomy was performed at the thoracic 9–10 (T9-T10) level after shaving the back and neck, exposing the cord beneath without the dura disruption. The exposed spinal cord was subjected to moderate injury (10 g x 25 mm) using a New York University (NYU) impactor as previously described [19]. Rats also underwent laminectomy at T9-T10 level without injury for sham control. All animal experiments were performed in accordance with the Guidelines of Animal Care Committee of the Kyung Hee University (permission number: KHUASP(SE)-17-059).

Endothelial Cell Culture and OGD/Reperfusion

American Type Culture Collection (Manassas, VA) provided a mouse brain endothelial cell line (bEnd.3), which was cultured as previously described [20, 21]. bEnd.3 cells was seeded onto 6-well plate with 5 x 10^5 cells in each well and subjected to oxygen glucose deprivation (OGD) in a humidified anaerobic chamber (APM-30D, Astec, Fukuoka, Japan) as previously described (Park et al., 2020). Then, cells were

replaced under normoxic conditions and the media was changed with 25 mM glucose containing DMEM. Under normoxic condition, control cells were also cultured in DMEM with 25 mM glucose.

In vitro and in vivo drug administration

CAR (5-isopropyl-2-methylphenol, Sigma-Aldrich, St. Louis, MO) was dissolved in 0.9% saline. For in *vitro* study, CAR (500 μM) was treated for 30 min before OGD. For control, 0.9% saline without drugs was used. For *in vivo* study, CAR (50 mg/kg) dissolved in 0.9% saline was infected intraperitoneally (i.p.) into injured rats immediately and 8 h after injury and then further administered once a day for 7 d for behavioral tests or for indicated time points for other experiments. 0.9% saline was injected for vehicle group. Sham-operated control rats did not receive any pharmacological treatment.

Measurement of BSCB disruption

As previously described, the permeability of the BSCB was measured using Evans blue dye extravasation [22]. In brief, Evans blue dye (Sigma) was dissolved in 0.9% saline and 5 ml of dye (2 %) was injected via i.p. at 1 d after SCI. The rats were sacrificed three hours later via intra-cardiac perfusion with PBS. The T9 spinal cords segment (1 cm) with lesion epicenter was removed and homogenized in a 50% trichloroacetic acid solution. The level of Evans blue was determined by spectrophotometer (Molecular device, Sunnyvale, CA) at 620 nm (excitation wavelength) and 680 nm (emission wavelength). The quantity of Evans blue Dye in the sample was calculated by plotting a standard curve with known amounts of dye (micrograms/gram of tissue).

Tissue preparation

Injured rats were anesthetized at indicated time points with chloral hydrate and perfused with 0.1 M PBS and then with 4% paraformaldehyde in 0.1 M PBS. The spinal cord (10 mm) was dissected out and post-fixed by immersing it in the same fixative for 5 h and placing it in 30% sucrose in 0.1 M PBS. After embedding the spinal segment for frozen sections, longitudinal or transverse sections were cut on a cryostat at 10 or 20 μm (CM1850; Leica, Germany). For molecular work, the spinal cord segment (1 cm) with the lesion epicenter were also isolated after perfusion with 0.1 M PBS and frozen at -80°C.

RNA isolation and RT-PCR

TRIZOL Reagent (Invitrogen) was used to prepare total RNA, and 1 μg of total RNA was reverse-transcribed into first strand cDNA using MMLV according to the manufacturer's instructions (Invitrogen) as described [22]. The resulting cDNAs were subjected to RT- PCR using a thermal cycler (Takara Bio, Shiga, Japan). The primers used for *Trpm7, Il-6, Tnf-α, Cox-2, inos, Mcp-1, Mip-1α, Mip-1β, Gro-α, Mip-2α* and *Gapdh* were synthesized by the Genotech (Daejeon, Korea) and the primer sequences are shown in Table 1. PCR products were separated using agarose gel electrophoresis (1.5 or 3 %) and stained with ethidium bromide. The relative band intensity was measured by the AlphaImager software (Alpha Innotech Corporation) and compared to sham control value. The relative intensity values from three times of experiments were subjected to statistical analysis.

Western blot

Total protein was isolated using a lysis buffer (1% Nonidet P-40, 20 mM Tris, pH 8.0, 137 mM NaCl, 0.5 mM EDTA, 10% glycerol, 10 mM $Na_2P_2O_7$, 10 mM NaF, 1 μg/ml aprotinin, 10 μg/ml leupeptin, 1 mM vanadate, and 1 mM PMSF) as described previously [22]. SDS-PAGE was used to separate protein samples (30 μg) and transfer them to nitrocellulose membrane (Millipore, Billerica, MA). The membranes were incubated for 1 h at room temperature with blocking solution (Tris-buffered saline containing 0.1 % tween-20 and 5% skim milk or bovine serum albumin), then overnight at 4°C with primary antibodies listed in Table 2. Secondary antibodies conjugated with horseradish peroxidase (Jackson ImmunoResearch, West Grove, PA) were used to detect the primary antibodies and immunoreactive bands were visualized using chemiluminescence (Thermo Scientific, Rockford, IL). Immunoblot image and the densitometirc values were obtained by using AlphaImager software (Alpha Innotech Corporation, San Leandro, CA). β-tubulin was normalized to internal standard.

Immunohistochemistry

Frozen sections were processed for immunohistochemistry as previously described [23] using antibodies against TRPM7, neuronal-specific nuclear protein (NeuN), CC1, RECA1, ZO-1, myeloperoxidase (MPO), ED-1, and cleaved caspase-3, which are listed in Table 2. Fluorescein isothiocyanate (FITC)- or cyanin 3-conjugated secondary antibodies (Jackson Immunoresearch) was used for double labeling. The manufacturer's protocol was used to label nuclei with DAPI (Molecular Probes). Serial transverse sections were collected every 100 or 200 m section rostral and caudal 3,000 or 4,000 m to the lesion site to quantify MPO or ED-1 intensity and cleaved caspase-3-positive oligodendrocytes (cleaved caspase-3/CC1 double-positive) (total 40 or 60 sections). Digital images of MPO, ED-1-stained tissues, and cleaved caspase-3/CC1 double-positive oligodendrocytes in the WM were obtained and quantified using MetaMorph software (Molecular device) as previously described [22]. The value was normalized to the primary antibody omitted control after the threshold value and backgrounds were quantified. Serial sections were also stained with Cresyl violet acetate for histological analysis.

Measurement of transendothelial electrical resistance (TEER)

Endothelial permeability was determined by measuring TEER according to the manufacturer's instructions (Millipore) as described [22, 23]. Briefly, bEnd.3 cells were seeded (5 x 10^5 cells) and seeded and cultured for 24 h on Transwell inserts (Transwell-COL, Corning) coated with rat tail collagen. Cells were than subjected to OGD/reperfusion injury and TEER was determined using with a Millicell ERS-2 Volt-Ohm Meter (Millipore). The surface area of the Transwell inserts was used to calculate the values in ohms per square centimeter ($\Omega \cdot cm^2$).

Cell counting of viable ventral motor neuron (VMN)

Serial transverse spinal cord sections (20 m thickness) were collected every 500 m section rostral and caudal 8 mm to the lesion site and stained with Cresyl violet acetate to count the number of viable motor

neurons (VMN). VMN located in the lower ventral horn and larger than half the size of the sampling square (20 x 20 μm) was manually counted and analyzed using MetaMorph software (Molecular Device) as described [22].

TUNEL staining

TUNEL staining was performed on injured spinal cord (1 and 5 d after injury) serial transverse sections (20 μm thickness) collected every 200 μm interval using an Apoptag in situ kit (Millipore) according to the manufacturer's instructions. TUNEL-positive cells with morphological features of nuclear condensation and/or compartmentalization in gray matter (GM) at 1 d and white matter (WM) at 5 d after injury were counted and quantified as described in the previous report [22, 24]. All TUNEL analyses were performed by investigators who were unaware of the experimental conditions.

Behavioral tests

Behavioral tests including Basso-beattie-Bresnahan (BBB), inclined plane test, grid walk, and foot print were performed according to previously described [25–28]. Basso-Beattie-Bresnahan (BBB) locomotion scale, which is a 22-point scale (scores 0–21) was used to evaluate hindlimb locomotor function. For the inclined plane test, rats were placed on the testing apparatus in one of two positions (right side or left side up), and the maximum angle maintained without falling for 5 s was recorded and averaged. Rats were also tested on a horizontal grid to assess their ability to precisely place the hindlimb, and the number of footfalls (mistakes) in foot placement were counted. For the footprint analysis, both forepaws and hindpaws were dipped in nontoxic red and blue dye before walking across a narrow box (1 m long and 7 cm wide). The footprints were then scanned, and resulting digitized images were examined. Behavioral analyses were carried out by trained investigators who were unaware of the experimental conditions.

Histological analysis of myelin and axon

Rats were perfused after behavioral tests (35 days after injury) for histological analyses, and frozen sections were prepared as described above. For axon density quantification, serial transverse sections were stained with an antibody specific for 200 kDa neurofilament protein (NF200, 1:4,000; Sigma) and axon density within preselected fields (40 × 40 μm, 1,600 μm^2) at specific sites within the ventral and dorsolateral funiculi was determined as previously described [25]. Some sections were stained with 5-hydroxytryptamine (5-HT, 1:5,000; Diasorin, Stillwater, MN) and the ABC method was used to detect labeled cells using a Vectastain kit (Vector Laboratories). Selected slides were stained with 0.1 % Luxol fast blue (Solvent Blue 38; Sigma) in acidified 95 % ethanol and incubated overnight at 60°C for myelin staining. The differentiation step was then carried out with 0.05 % lithium carbonate, as previously described [29]. MetaMorph software (Molecular Device) was used to create digital images of Luxol fast blue-stained tissues.

Measurement of lesion volume

As previously described, serial longitudinal sections from rats tested for behavioral analyses were used to measure lesion volume [30]. Every 50 μm section was stained with Cresyl violet acetate and the lesion volume was calculated by measuring the area of cavitation at the injury epicenter with a low-power (1.25 x) objective and then using a MetaMorph software (Molecular Device).

Statistical analysis

The data were presented as the mean, standard deviation, or standard error of the mean (SEM). To determine the statistical significance of the difference between the vehicle- and CAR-treated groups, the unpaired Student's *t* test was used. For immunohistochemical, and molecular analyses comparisons were based on a one-way ANOVA. BBB locomotor scale and inclined plane test were analyzed using repeated measurement ANOVA (time vs treatment) with post-hoc Tukey's multiple comparison. SPSS 15.0 (SPSS Science, Chicago, IL) was used for statistical analysis. $P < 0.05$ was considered to be statistically significance.

Results

The expression of TRPM7 is up-regulated after SCI

In the event of cerebral ischemia and hypoxia, ionic imbalances, including calcium overload inside the neuronal cells, are the established cellular and molecular mechanisms for ischemia and hypoxic neuronal cell death followed brain damage [31]. An *in vivo* study also showed that the expression of TRPM7 was increased in hippocampal neurons through PI-3K signal pathway after middle cerebral artery occlusion model (MCAO) [32].

To test the hypothesis that TRPM7 channels may contribute to biological events following SCI, we first examined the profile of TRPM7 expression in injured rat spinal cords. TRPM7 expression was markedly up-regulated after SCI (Fig. 1A and B). RT-PCR and Western blot analysis revealed that TPRM7 expression was increased and peaked at 7 d after SCI. TRPM7 was also mainly localized in neurons in the GM and oligodendrocytes in the WM, in the uninjured rat spinal cord (Fig. 1C, Sham). By double-immunofluorescence analysis, TRPM7 was colocalized in neurons (NeuN) and oligodendrocytes (CC1), respectively (Fig. 1D, Sham). Interestingly, TRPM7 expression was increased in the blood vessels at or near the lesion site in the injured spinal cord (Fig. 1C, 7d). Consistent with these results, this up-regulation of TRPM7 expression was not observed in the blood vessels of uninjured spinal cords (Fig. 1D, Sham) and majority of TRPM7-positive blood vessels in the injured spinal cord were also positive for the endothelial cell marker RECA1 (Fig. 1D, 7d). These results indicate that TRPM7 is up-regulated in the blood vessels after SCI.

CAR inhibits BSCB disruption and preserves tight junction (TJ) integrity after injury

It is well known that SCI causes in the breakdown of the BSCB [33], and blocking BSCB disruption enhances functional recovery by alleviating the infiltration of blood cells including neutrophils and

macrophages followed inflammatory responses [21]. To determine whether ion influx through TRPM7 affects the BSCB disruption, we evaluated the effect of CAR, a TRPM7 inhibitor, on BSCB disruption at 1 d after injury by Evans blue assay. Compared with sham group, the amount of Evans blue dye extravasation was markedly increased at 1d after SCI, implying BSCB leakage (Fig. 2A). Furthermore, CAR administration significantly reduced the amount of Evans blue dye extravasation at 1 d after SCI as compared with the vehicle group (Veh 72.69 ± 5.05 vs. CAR 15.61 ± 2.51 μg/g tissue, $p < 0.05$). Next, we examined the effect of CAR on the TJ protein levels of ZO-1 and occludin at 4 h and 5 d after injury. As shown in Fig. 2B, CAR significantly attenuated the decrease in TJ protein levels after injury compared with the vehicle control (ZO-1, Veh 0.68 ± 0.04 vs. CAR 0.94 ± 0.04; occludin, Veh 0.62 ± 0.03 vs. CAR 0.94 ± 0.07, $p < 0.05$). In addition, double immunofluorescence staining for ZO-1 and RECA-1 showed that the fragmentation of capillary blood vessel was increased after SCI and ZO-1 immunoreactivity was decreased upon injury, compared with the sham control, whereas CAR treatment attenuated the fragmentation of the capillary blood vessels and ZO-1 loss (Fig. 2C), indicating that TRPM7 affected TJ integrity and BSCB disruption upon SCI.

TRPM7 is also up-regulated and regulates the integrity of TJ in OGD-induced bEnd.3 cells

To understand more about the molecular mechanism underlying TRPM7-mediated regulation in injured blood vessels, an *in vitro* OGD/reperfusion model with a bEnd.3 mouse brain microvessel endothelial cell line was used. Under the optimized condition of OGD/reperfusion injury to induce the maximal expression of the TRPM7 gene in bEnd.3 cells (data not shown), the expression of the TRPM7 mRNA and protein was increased in the bEnd.3 cells subjected to 6 h of OGD treatment followed by 0.5 h, 1 h, and 3 h of reperfusion (Fig. 3A and B). By Western blot analysis with anti-ZO-1 and occludin antibodies, the expression of the TJ proteins, ZO-1 and occludin, was decreased in the OGD/reperfusion injury-induced bEnd.3 cells (Fig. 3C, +OGD). However, CAR substantially attenuated the decrease in ZO-1 and occludin expression in the bEnd.3 cells after OGD/reperfusion injury (Fig. 3C, +OGD/CAR) (ZO-1, +OGD 0.6 ± 0.03 vs. +OGD/CAR 1.0 ± 0.04; occludin, +OGD 0.7 ± 0.07 vs. +OGD/CAR 0.9 ± 0.04, $p < 0.05$). Consistently, trans-endothelial electrical resistance (TEER) was decreased in the OGD/reperfusion injury-induced bEnd.3 cells compared with the untreated control (Fig. 3D, +OGD). In parallel with these results, the decrease of TEER by OGD/reperfusion injury was significantly inhibited by CAR treatment (Fig. 3D, +OGD/CAR) (+ OGD 35 ± 6 vs. +OGD/CAR 72 ± 7, $p < 0.05$). These results indicate that TRPM7 affects TJ integrity by increasing the degradation of TJ molecules.

CAR inhibits the infiltration of neutrophils and macrophages and the expression of inflammatory factors after SCI

BSCB disruption and blood cell infiltration after SCI are known to mediate inflammatory responses, thereby contributing to the secondary injury cascade by releasing inflammatory mediators such as *Il-6, Tnf-a, Cox-2*, and *iNos* [20, 34, 35]. Furthermore, the early increase in chemokines such as *Mcp-1, Mip-1β, Gro-α*, and *Mip-2α* following SCI is considered to cause neutrophil and macrophage infiltration, thus facilitating inflammatory responses [36–39]. Since CAR prevented BSCB disruption following, the effect

of CAR treatment on blood cell infiltration was examined by immunofluorescence staining and Western blot with neutrophil and macrophage cell markers, MPO and ED-1 antibodies. Immunofluorescence staining showed that numerous MPO-positive cells (after 1 d) and ED-1-positive cells (after 5 d) were observed in the dorsal column of the injured spinal cord. However, CAR treatment attenuated the infiltration of these cells compared with the infiltration into the vehicle control (Fig. 4A and B). Additionally, relative fluorescence intensity analysis revealed that CAR treatment significantly reduced the infiltration of blood cells compared with that of the vehicle control (MPO, Veh 1.0 ± 0.07 vs. CAR 0.6 ± 0.05; ED-1, Veh 1.0 ± 0.02 vs. CAR 0.5 ± 0.08, $p < 0.05$). By Western blot and quantitative analyses, the level of ED-1 was markedly increased after SCI and was significantly attenuated by CAR treatment (Fig. 4C) (Veh 1.0 ± 0.07 vs. CAR 0.6 ± 0.06, $p < 0.05$). These findings suggest that the inhibition of TRPM7 reduced the infiltration of blood cells by preventing BSCB disruption after SCI.

Next, RT-PCR and Western blot tests were used to look at the effect of CAR on the expression of inflammatory mediators and chemokines after SCI. The results revealed that the increases CAR inhibited the increases in *Tnf-α*, *IL-1β* (at 2 h), *IL-6, Cox-2*, and *iNos* (at 6 h) mRNA levels after SCI (Fig. 4D and E). Furthermore, CAR suppressed the increases in the mRNA levels of *Mcp-1, Mip-1α, Mip-1β, Gro-α* (at 2 h), and *Mip-2α* (at 6 h) following injury (Fig. 4F and G). CAR also decreased COX-2 and iNOS protein levels at 1 d after injury as compared to vehicle control (Fig. 4H).

CAR inhibits the apoptotic cell death of neurons and oligodendrocytes

TRPM7 is known to play an important role in neuronal cell death in various neurodegenerative disease models, including SCI [10, 12, 18]. Furthermore, after BSCB damage, infiltrated blood cells such as neutrophils and macrophages are known to produce inflammatory mediators such as cytokines and chemokines, which contribute to cell death [40–42]. Thus, based on our results showing that TRPM7 is involved in the BCSB disruption after SCI, we next examined whether CAR inhibits apoptotic cell death by attenuating inflammatory responses following BSCB disruption. As previously mentioned, a massive loss of VMN was observed in the lesion area following injury [30], when compared to the vehicle control, CAR treatment reduced VMN loss both rostral and caudal to the lesion epicenter (Fig. 5A). The cleaved caspase-3-positive cells in the WM 5 days after SCI were CC1-positive oligodendrocytes, according to double immunofluorescence staining. Immunofluorescence with cleaved anti-caspase-3 antibody showed that CAR treatment significantly decreased the number of active caspase-3-positive cells in the WM at 5 d after injury as opposed to the vehicle control (Fig. 5B and C) (Veh 221 ± 16 vs. CAR 141 ± 11; $p < 0.05$). By Western blot, CAR treatment significantly reduced the levels of cleaved caspase-3 at 1 d and 5 d after injury compared with the vehicle control (Fig. 5D and E) (1 d, Veh 4.1 ± 0.4 vs. CAR 2.2 ± 0.4; 5 d, Veh 4.9 ± 0.4 vs. CAR 2.0 ± 0.3 $p < 0.05$).

Next, by TUNEL staining of spinal tissue at 1 d and 5 d after SCI, TUNEL-positive cells were also observed within the lesion site in the GM at 1 d and outside the lesion area (WM) at 5 d. Consistent with our previous reports [24, 43], the majority of TUNEL-positive cells in the GM at 1 d were identified as neurons. TUNEL-positive cells in the WM at 5 d were also observed outside of the lesion area, extending the entire

length of the section (20 mm) and were known as oligodendrocytes. As shown in Fig. 5F and G, CAR treatment resulted in a significant reduction in the number of TUNEL-positive cells when compared with the vehicle control in the GM at 1 d and the WM at 5 d (1 d, Veh 405 ± 36 vs. CAR 262 ± 4; 5 d, Veh 325 ± 12.2 vs. CAR 185 ± 8.3, $p < 0.05$). As a result, our findings show that inhibiting TRPM7 with CAR prevents apoptotic cell death in neurons and oligodendrocytes following injury.

CAR increases functional recovery after SCI

To assess the effect of CAR on functional recovery, CAR (50 mg/kg, i.p) was administered immediately and 8 hours after injury and then once daily for 7 days. Functional recovery was assessed 28 d after injury using BBB scale, inclined plane test, grid, and footprint analysis. As shown in Fig. 6A, CAR significantly improved hindlimb locomotor function from 14 d to 35 d after injury compared with the vehicle group (At 28 d, CAR 11.8 ± 1.1 vs. Veh 8.8 ± 0.9, $p < 0.05$). Furthermore, the ability to control and accurately position the hindlimbs was checked on a horizontal grid at 28 d after injury. From 14 to 28 days after damage, the angle of the incline was significantly higher in the CAR-treated rats than in the vehicle group (Fig. 6B) (At 28 d, CAR 66.3 ± 3.1 vs. Veh 55 ± 2.7 %, $p < 0.05$). As shown in Fig. 6C, the number of mistakes (footfalls on the grid walk) was significantly smaller in the CAR-treated group than in the vehicle group (At 28 d, CAR 43 ± 1.9 vs. Veh 73.6 ± 4.2, $p < 0.05$). Finally, footprint examination indicated that fairly consistent forelimb-hindlimb coordination was observed in both the vehicle-treated and CAR-treated rats at 35 d after SCI, but CAR-treated group was very little toe dragging, compared to inconsistent dorsal stepping and extensive dragging in the vehicle rats, as revealed by ink streaks extending from both hindlimbs (Fig. 6D).

CAR decreases lesion volume and inhibits the loss of axon and myelin after SCI

We performed a histological study of the spinal cord tissues from the animals used in the behavioral tests to confirm the correlation between the behavioral results and histological results such as axon loss, myelin loss, and lesion volume. To determine whether CAR retains axons after injury, immunostaining with anti-NF200 and anti-5-HT antibodies was used to detect the remaining axons, and the density of the preserved axons was measured as described in the Materials and Methods section. In the sham control, NF200-positive axons were dense and axonal packing was uniform in both the ventral and dorsolateral funiculi (Fig. 7A and B, Sham). However, the axon density was significantly decreased in the injured tissue (Fig. 7A and B, Veh). The number of NF200-positive axons was significantly higher in the CAR-treated group than in the vehicle control group in both the ventral and dorsolateral funiculi (Fig. 7A and B) (rostral 2 mm, ventral funiculus, CAR 61 ± 5.3 vs. Veh 26 ± 5.4 %; dorsolateral funiculus, CAR 57 ± 5.3 vs. Veh 29 ± 6.0 %, $P < 0.05$). Furthermore, the density of the 5-HT serotonergic axons in the ventral horn was higher in the CAR-treated group than in the vehicle control (Fig. 7C). These findings imply that CAR treatment reduces axon loss following SCI.

Next, the extent of myelin loss after injury was assessed by Luxol fast blue staining. At 35 d after injury, extensive myelin loss near the lesion area was evident in the vehicle-treated group but not in the sham control (Fig. 7D, Veh); however, CAR treatment attenuated myelin loss (Fig. 7D, CAR). Serial longitudinal

sections were stained with Cresyl violet and the lesion volume was assessed to evaluate the tissue loss after SCI. Figure 7E reveals that the overall lesion volume was significantly reduced in the CAR-treated group compared to the vehicle-treated group at 35 d after injury (Fig. 7E) (CAR 4.5 ± 0.3 vs. Veh 7.6 ± 0.9 mm^3, $P < 0.05$).

Discussion

In this study, we demonstrated that TRPM7, a calcium-mediated non-selective divalent cation channel, plays a critical role in BSCB disruption after SCI. Both in vitro and in vivo studies have shown that the expression of TRPM7 was increased in the endothelial cells consisting of BSCB after SCI. In addition, CAR suppressed BSCB disruption by inhibiting the loss of TJ proteins and preserved the TJ integrity after SCI, suggesting that blocking the TRPM7 channel can inhibit the destruction of the BSCB. CAR also decreased the blood cell infiltration such neutrophils and macrophages following SCI, thereby inhibiting the expression of inflammatory factors such as TNF-α, IL-6, COX-2, iNOS and chemokines such as *Mcp-1, Mip-1α, Mip-1β, Gro-α*, and *Mip-2α*, resulting in reduced inflammatory responses. CAR treatment decreased apoptotic cell death in neurons and oligodendrocytes and increased functional recovery after SCI. Thus, our findings suggest that TRPM7 is a potential target in therapeutic drug development for use in SCI.

The normal function of the spinal cord is dependent on the microenvironment. The breakdown of the BSCB after SCI induces changes in the spinal microenvironment by facilitating immune cells infiltration into the spinal cord [33] and triggers the post-traumatic inflammatory response, which results in additional spinal cord damage. MMP-9 upregulation is linked to BSCB disruption because it degrades the basal components of BSCB, such as TJ proteins. Furthermore, blood brain barrier (B-BB) disruption was reduced in MMP-9 knockout mice after cerebral ischemia by reducing the protein degradation of ZO-1 relative to wild type mice [44]. Furthermore, our recent studies have shown that inhibiting MMP-9 expression and activation significantly reduces BSCB disruption [29, 35, 45]. Specially, we recently found that Jmjd3, histone H3K27 demethylase, plays a important role as an epigenetic regulator in MMP-9 expression in vascular endothelial cells after SCI [23]. CAR treatment significantly prevented BSCB disruption, according to our findings. TJ proteins were also degraded after SCI, but CAR treatment retained these molecules considerably. However, it is not yet known how the inhibition of TRPM7 prevents BSCB disruption after SCI. The precise mechanism underlying TRPM7-mediated inhibition of BSCB disruption after SCI will be investigated in a future study.

Reactive oxygen species (ROS) have play critical roles in the apoptotic cell death after SCI [30, 46]. After injury, The accumulation of free radicals such as superoxide anion ($O_2\bullet^-$), hydroxyl radical, and peroxynitrite triggered apoptotic cell death [47]. Furthermore, it was reported that nitric oxide and peroxynitrite play important roles in the B-BB disruption and endothelial cell permeability [48, 49]. Via the RhoA, phosphatidylinositol 3 kinase, and protein kinase B (PKB/AKT) signaling pathways, superoxide anion has also been shown to control endothelial TJ proteins and improve B-BB permeability [49]. The report by Jiang et al. [18] showed that carvacrol exhibits a neuroprotective effect after SCI by inhibiting

oxidative stress and the eNOS signaling pathway. It was also reported that the application of 2-aminoethoxy-diphenyl borate (2-APB), an inhibitor of TRPM7, or knockdown of TPRM7, protects the neurons from $H_2O_2^-$ mediated injury [50]. Thus, we cannot exclude the possibility that carvacrol has a direct neuroprotective effect or the possibility that it prevents BSCB breakdown via its antioxidant effects, although we focused on the role of TRPM7 in the disruption of BSCB after SCI in this study. Future studies will be performed to elucidate the precise mechanism underlying TRPM7-mediated cell death and BSCB disruption by ROS after SCI.

Inflammation plays a critical role in the secondary damage caused by SCI. BSCB disruption after injury leads to the cell infiltration into the spinal cord parenchyma. These infiltrated immune cells produce inflammatory factors, causing tissue injury, triggering cell death, and impairing locomotor behavior after SCI [51–53]. Several studies have also shown that inhibiting neutrophils and macrophages infiltration after injury reduces apoptotic cell death and improves functional recovery [54, 55]. In this study, we found that the neuroprotective effect of CAR is mediated by inhibiting BSCB disruption and the infiltration of inflammatory cells after SCI, which alleviates apoptotic cell death and improves functional recovery. However, according to previous studies, TRPM7 is expressed in neurons or oligodendrocytes [10]. Furthermore, our data showed that TRPM7 is expressed in neurons and oligodendrocytes in the uninjured and injured spinal cord. Thus, it is possible that the neuroprotective effect of CAR can be mediated by directly affecting the ion influx into neurons and oligodendrocytes, and this possibility will be examined in a future study.

In summary, our findings suggest an important role for TRPM7 and its potential mechanisms in BSCB disruption, which might aid in gaining further understanding of BSCB disruption and cell death after SCI.

Declarations

Funding

This work was supported by the National Research Foundation of Korea (NRF) grant funded by the Korea government (MSIT, No. NRF-2019R1A2C2003750) and by the Brain Research Program through the National Research Foundation of Korea funded by the Korean Government (MIST; 2017M37A1025369) to T.Y.Y. J.Y.L is a recipient of funding from the National Research Foundation of Korea (NRF) grant funded by the Korea government (MSIT, No. NRF-2019R1A2C1005791).

Conflict of Interest

The authors declare no competing interests.

Contributions

C.S.P., J.Y.L., B.G.J. and T.Y.Y. designed the research. C.S.P, H.Y.C and J.Y.L. performed the experiments and analyzed the data. C.S.P., J.Y.L., and T.Y.Y. wrote the manuscript.

Availability of data and material

The data that support the findings of this study are available from the corresponding author on request.

Code availability

Not applicable

Ethics Approval

Animal care and handling were performed in accordance with the laboratory's standard operating procedures and were accredited by the Animal Care Committee of the Kyung Hee University (permission number: KHUASP(SE)-17-059).

Consent to Participate

Not applicable

Consent for Publication

Not applicable

Compliance with Ethical Standards

Disclosure of potential conflicts of interest

The authors declare no competing interests.

Research involving Human Participants and/or Animals

We used adult male Sprague-Dawley rats (250-300 g, Samtako, Osan, Korea) in this study. Animal care and handling were performed in accordance with the laboratory's standard operating procedures and were accredited by the Animal Care Committee of the Kyung Hee University (permission number: KHUASP(SE)-17-059).

Informed consent

Not applicable

References

1. Bennett J, Emmady JMD PD. Spinal Cord Injuries. In: *StatPearls.* (Treasure Island (FL), 2020)
2. Ham TR, Leipzig ND (2018) Biomaterial strategies for limiting the impact of secondary events following spinal cord injury. Biomed Mater 13:2:024105

3. Kumar H, Ropper AE, Lee SH, Han I (2017) Propitious Therapeutic Modulators to Prevent Blood-Spinal Cord Barrier Disruption in Spinal Cord Injury. Mol Neurobiol 54:5:3578–3590
4. Young W (1985) The role of calcium in spinal cord injury. Cent Nerv Syst Trauma 2:2:109–114
5. Thakore P, Earley S (2019) Transient Receptor Potential Channels and Endothelial Cell Calcium Signaling. Compr Physiol 9:3:1249–1277
6. Smani T, Gomez LJ, Regodon S et al (2018) TRP Channels in Angiogenesis and Other Endothelial Functions. Front Physiol 9:1731
7. Venkatachalam K, Montell C (2007) TRP channels. Annu Rev Biochem 76:387–417
8. Jin J, Desai BN, Navarro B et al (2008) Deletion of Trpm7 disrupts embryonic development and thymopoiesis without altering Mg2 + homeostasis. Science 322:5902:756–760
9. Inoue K, Branigan D, Xiong ZG (2010) Zinc-induced neurotoxicity mediated by transient receptor potential melastatin 7 channels. J Biol Chem 285:10:7430–7439
10. Visser D, Middelbeek J, van Leeuwen FN, Jalink K (2014) Function and regulation of the channel-kinase TRPM7 in health and disease. Eur J Cell Biol 93:10–12:455–465
11. Sun Y, Sukumaran P, Schaar A, Singh BB (2015) TRPM7 and its role in neurodegenerative diseases. Channels 9:5:253–261
12. Aarts M, Iihara K, Wei WL et al (2003) A key role for TRPM7 channels in anoxic neuronal death. Cell 115:7:863–877
13. Aarts MM, Tymianski M (2005) TRPM7 and ischemic CNS injury. Neuroscientist 11:2:116–123
14. Chen W, Xu B, Xiao A et al (2015) TRPM7 inhibitor carvacrol protects brain from neonatal hypoxic-ischemic injury. Mol Brain 8:11
15. Sun HS, Jackson MF, Martin LJ et al (2009) Suppression of hippocampal TRPM7 protein prevents delayed neuronal death in brain ischemia. Nat Neurosci 12:10:1300–1307
16. Landman N, Jeong SY, Shin SY et al (2006) Presenilin mutations linked to familial Alzheimer's disease cause an imbalance in phosphatidylinositol 4,5-bisphosphate metabolism. Proc Natl Acad Sci U S A 103:51:19524–19529
17. Hermosura MC, Garruto RM (2007) TRPM7 and TRPM2-Candidate susceptibility genes for Western Pacific ALS and PD? Biochim Biophys Acta 1772:8:822–835
18. Jiang ZS, Pu ZC, Hao ZH (2015) Carvacrol protects against spinal cord injury in rats via suppressing oxidative stress and the endothelial nitric oxide synthase pathway. Mol Med Rep 12:4:5349–5354
19. Lee SM, Yune TY, Kim SJ et al (2003) Minocycline reduces cell death and improves functional recovery after traumatic spinal cord injury in the rat. J Neurotrauma 20:10:1017–1027
20. Lee K, Na W, Lee JY et al (2012) Molecular mechanism of Jmjd3-mediated interleukin-6 gene regulation in endothelial cells underlying spinal cord injury. J Neurochem 122:2:272–282
21. Lee JY, Kim HS, Choi HY, Oh TH, Yune TY (2012) Fluoxetine inhibits matrix metalloprotease activation and prevents disruption of blood-spinal cord barrier after spinal cord injury. Brain 135:pt 8:2375–2389

22. Park CS, Lee JY, Choi HY et al (2020) Gallic acid attenuates blood-spinal cord barrier disruption by inhibiting Jmjd3 expression and activation after spinal cord injury. Neurobiol Dis 145:105077
23. Lee JY, Na WH, Choi HY et al (2016) Jmjd3 mediates blood-spinal cord barrier disruption after spinal cord injury by regulating MMP-3 and MMP-9 expressions. Neurobiol Dis 95:66–81
24. Lee JY, Chung H, Yoo YS et al (2010) Inhibition of apoptotic cell death by ghrelin improves functional recovery after spinal cord injury. Endocrinology 151:8:3815–3826
25. Yune TY, Lee JY, Jung GY et al (2007) Minocycline alleviates death of oligodendrocytes by inhibiting pro-nerve growth factor production in microglia after spinal cord injury. J Neurosci 27:29:7751–7761
26. Merkler D, Metz GA, Raineteau O et al (2001) Locomotor recovery in spinal cord-injured rats treated with an antibody neutralizing the myelin-associated neurite growth inhibitor Nogo-A. J Neurosci 21:10:3665–3673
27. Basso DM, Beattie MS, Bresnahan JC (1995) A sensitive and reliable locomotor rating scale for open field testing in rats. J Neurotrauma 12:1:1–21
28. Rivlin AS, Tator CH (1977) Objective clinical assessment of motor function after experimental spinal cord injury in the rat. J Neurosurg 47:4:577–581
29. Lee JY, Choi HY, Park CS, Ju BG, Yune TY (2018) Mithramycin A Improves Functional Recovery by Inhibiting BSCB Disruption and Hemorrhage after Spinal Cord Injury. J Neurotrauma 35:3:508–520
30. Yune TY, Lee JY, Jiang MH et al (2008) Systemic administration of PEP-1-SOD1 fusion protein improves functional recovery by inhibition of neuronal cell death after spinal cord injury. Free Radic Biol Med 45:8:1190–1200
31. Sun HS (2017) Role of TRPM7 in cerebral ischaemia and hypoxia. J Physiol 595:10:3077–3083
32. Jiang H, Tian SL, Zeng Y, Li LL, Shi J (2008) TrkA pathway(s) is involved in regulation of TRPM7 expression in hippocampal neurons subjected to ischemic-reperfusion and oxygen-glucose deprivation. Brain Res Bull 76(1–2):124–130
33. Garcia E, Aguilar-Cevallos J, Silva-Garcia R, Ibarra A (2016) Cytokine and Growth Factor Activation In Vivo and In Vitro after Spinal Cord Injury. Mediators Inflamm 2016:9476020
34. Mun-Bryce S, Rosenberg GA (1998) Gelatinase B modulates selective opening of the blood-brain barrier during inflammation. Am J Physiol 274(5 Pt 2):R1203–R1211
35. Lee JY, Kim HS, Choi HY et al (2012) Valproic acid attenuates blood-spinal cord barrier disruption by inhibiting matrix metalloprotease-9 activity and improves functional recovery after spinal cord injury. J Neurochem 121:5:818–829
36. McTigue DM, Tani M, Krivacic K et al (1998) Selective chemokine mRNA accumulation in the rat spinal cord after contusion injury. J Neurosci Res 53:3:368–376
37. Ghirnikar RS, Lee YL, Eng LF (2001) Chemokine antagonist infusion promotes axonal sparing after spinal cord contusion injury in rat. J Neurosci Res 64:6:582–589
38. Ousman SS, David S (2001) MIP-1alpha, MCP-1, GM-CSF, and TNF-alpha control the immune cell response that mediates rapid phagocytosis of myelin from the adult mouse spinal cord. J Neurosci

21:13:4649–4656
39. Pineau I, Lacroix S (2007) Proinflammatory cytokine synthesis in the injured mouse spinal cord: multiphasic expression pattern and identification of the cell types involved. J Comp Neurol 500:2:267–285
40. Yang C, Hawkins KE, Dore S, Candelario-Jalil E (2019) Neuroinflammatory mechanisms of blood-brain barrier damage in ischemic stroke. Am J Physiol Cell Physiol 316(2):C135–C153
41. Zlokovic BV (2008) The blood-brain barrier in health and chronic neurodegenerative disorders. Neuron 57:2:178–201
42. Abbott NJ, Ronnback L, Hansson E (2006) Astrocyte-endothelial interactions at the blood-brain barrier. Nat Rev Neurosci 7:1:41–53
43. Yune TY, Lee JY, Cui CM, Kim HC, Oh TH (2009) Neuroprotective effect of Scutellaria baicalensis on spinal cord injury in rats. J Neurochem 110:4:1276–1287
44. Asahi M, Wang X, Mori T et al (2001) Effects of matrix metalloproteinase-9 gene knock-out on the proteolysis of blood-brain barrier and white matter components after cerebral ischemia. J Neurosci 21:19:7724–7732
45. Lee JY, Choi HY, Na WH, Ju BG, Yune TY (2014) Ghrelin inhibits BSCB disruption/hemorrhage by attenuating MMP-9 and SUR1/TrpM4 expression and activation after spinal cord injury. Biochim Biophys Acta 1842(12 Pt A):2403–2412
46. Bao F, Liu D (2002) Peroxynitrite generated in the rat spinal cord induces neuron death and neurological deficits. Neuroscience 115:3:839–849
47. Xu W, Chi L, Xu R et al (2005) Increased production of reactive oxygen species contributes to motor neuron death in a compression mouse model of spinal cord injury. Spinal Cord 43:4:204–213
48. Parathath SR, Parathath S, Tsirka SE (2006) Nitric oxide mediates neurodegeneration and breakdown of the blood-brain barrier in tPA-dependent excitotoxic injury in mice. J Cell Sci 119(Pt 2):339–349
49. Schreibelt G, Kooij G, Reijerkerk A et al (2007) Reactive oxygen species alter brain endothelial tight junction dynamics via RhoA, PI3 kinase, and PKB signaling. FASEB J 21:13:3666–3676
50. Coombes E, Jiang J, Chu XP et al (2011) Pathophysiologically relevant levels of hydrogen peroxide induce glutamate-independent neurodegeneration that involves activation of transient receptor potential melastatin 7 channels. Antioxid Redox Signal 14:10:1815–1827
51. Carlson SL, Parrish ME, Springer JE, Doty K, Dossett L (1998) Acute inflammatory response in spinal cord following impact injury. Exp Neurol 151:1:77–88
52. Beattie MS, Hermann GE, Rogers RC, Bresnahan JC (2002) Cell death in models of spinal cord injury. Prog Brain Res 137:37–47
53. Okada S, Nakamura M, Mikami Y et al (2004) Blockade of interleukin-6 receptor suppresses reactive astrogliosis and ameliorates functional recovery in experimental spinal cord injury. J Neurosci Res 76:2:265–276

54. Taoka Y, Okajima K, Uchiba M et al (1997) Role of neutrophils in spinal cord injury in the rat. Neuroscience 79:4:1177–1182
55. Saiwai H, Ohkawa Y, Yamada H et al (2010) The LTB4-BLT1 axis mediates neutrophil infiltration and secondary injury in experimental spinal cord injury. Am J Pathol 176:5:2352–2366

Tables

Table 1

Nucleotide sequences of primers and conditions used for RT-PCR

Target	Primer	Sequence
TRPM7	Forward	5’-GAATGGTCTGTGGAAAAGCACACG-3’
	Reverse	5’-CTTCTGCCCCATACTTTCCAAC-3’
IL-6	Forward	5'- TCACCATCTTCCAGGAGCGAGA-3'
	Reverse	5'- AGACGCCAGTAGACTCCACGAC-3’
TNF-α	Forward	5’-CCCAGACCCTCACACTCAGAT-3’
	Reverse	5’-TTGTCCCTTGAAGAGAACCTG-3’
COX-2	Forward	5’-CCATGTCAAAACCGTGGTGAATG-3’
	Reverse	5’-ATGGGAGTTGGGCAGTCATCAG-3’
iNOS	Forward	5’-CTCCATGACTCTCAGCACAGAG-3’
	Reverse	5’-GCACCGAAGATATCCTCATGAT-3’
MCP-1	Forward	5’-TCAGCCAGATGCAGTTAACG-3’
	Reverse	5’-GATCCTCTTGTAGCTCTCCAGC-3’
Mip-1α	Forward	5'-ACTGCCTGCTGCTTCTCCTACA-3'
	Reverse	5'-AGGAAAATGACACCTGGCTGG-3'
MIP-1β	Forward	5'-ACT GCC TGC TGC TTC TCC TAC A-3'
	Reverse	5’-GAATACCACAGCTGGCTTGGA-3’
Gro-α	Forward	5’-CCGAAGTCATAGCCACACTCAA-3’
	Reverse	5’-GCAGTCGTCTCTTTCTCCGTTAC-3’
MIP-2α	Forward	5’-AGACAGAAGTCATAGCCACTCTCAAG-3’
	Reverse	5’-CCTCCTTTCCAGGTCAGTTAGC-3’
GAPDH	Forward	5’-AACTTTGGCATTGTGGAAGG-3’
	Reverse	5’-GGAGACAACCAGGTCCTCAG’

Table 2
Antibody information for Western blot and IHC

Antibody	Manufacturer	Catalog number	Dilution used
TRPM7	Neuromab	9211	1:1000 for Western blot
TRPM7	Santa Cruz	SC-19562	1:100 for IHC
ZO-1	Invitrogen	40-2200	1:1000 for Western blot, 1:100 for IHC
Occludin	Invitrogen	404700	1:1000 for Western blot
ED-1	Serotec	MCA341R	1:1000 for Western blot, 1:100 for IHC
iNOS	BD Transduction	610333	1:1000 for Western blot
COX-2	Cayman chemical	160107	1:1000 for Western blot
Cleaved caspase-3	Cell Signaling Technology	9661	1:1000 for Western blot, 1:100 for IHC
β-tubulin	Sigma Aldrich	T4026	1:30000 for Western blot
NeuN	Millipore	MAB377	1:100 for IHC
CC1	abcam	ab16794	1:100 for IHC
RECA1	Santa Cruz	sc-542	1:100 for IHC
MPO	DAKO	A0398	1:100 for IHC

Figures

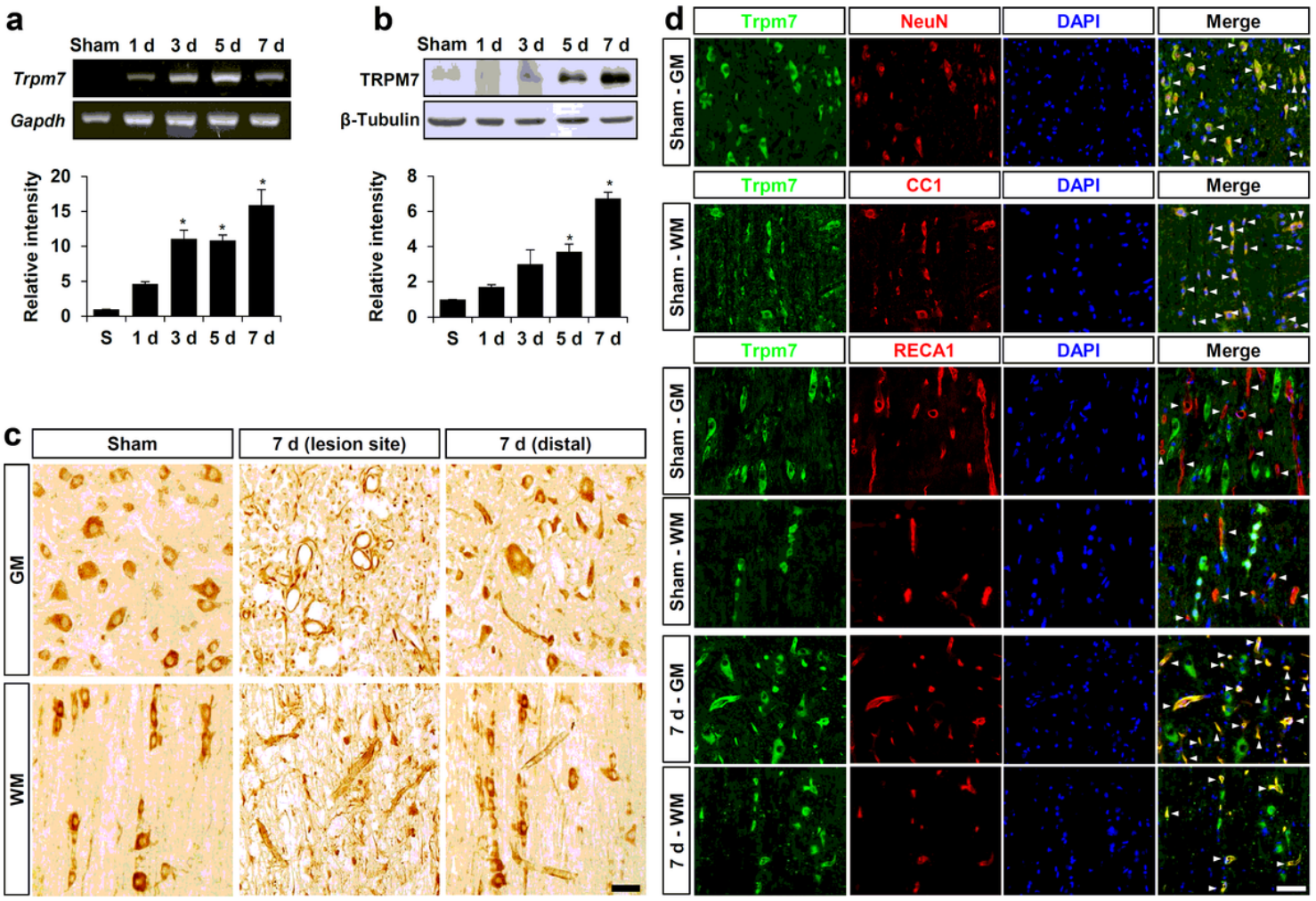

Figure 1

TRPM7 is up-regulated and expressed in blood vessel endothelial cells including neuron and oligodendrocyte after SCI. (A) RT-PCR and densitometric analysis for Trpm7 after injury (n = 5) (one-way ANOVA). (B) Western and densitometric analysis for TRPM7 after SCI (n = 5) (one-way ANOVA). (C) Immunohistochemistry of TRPM7 in sham and injured spinal cord (7 d). Scale bar = 50 mm. (D) Double immunofluorescence staining of TRPM7 with cell marker antibodies (NeuN for neuron, CC1 for oligodendrocyte, and RECA for blood vessel endothelial cell) in sham and injured spinal cord (7 d). Scale bar = 10 mm. All data represent mean ± SD. *p < 0.05 vs. vehicle (unpaired t-test). GM, gray matter; WM, white matter.

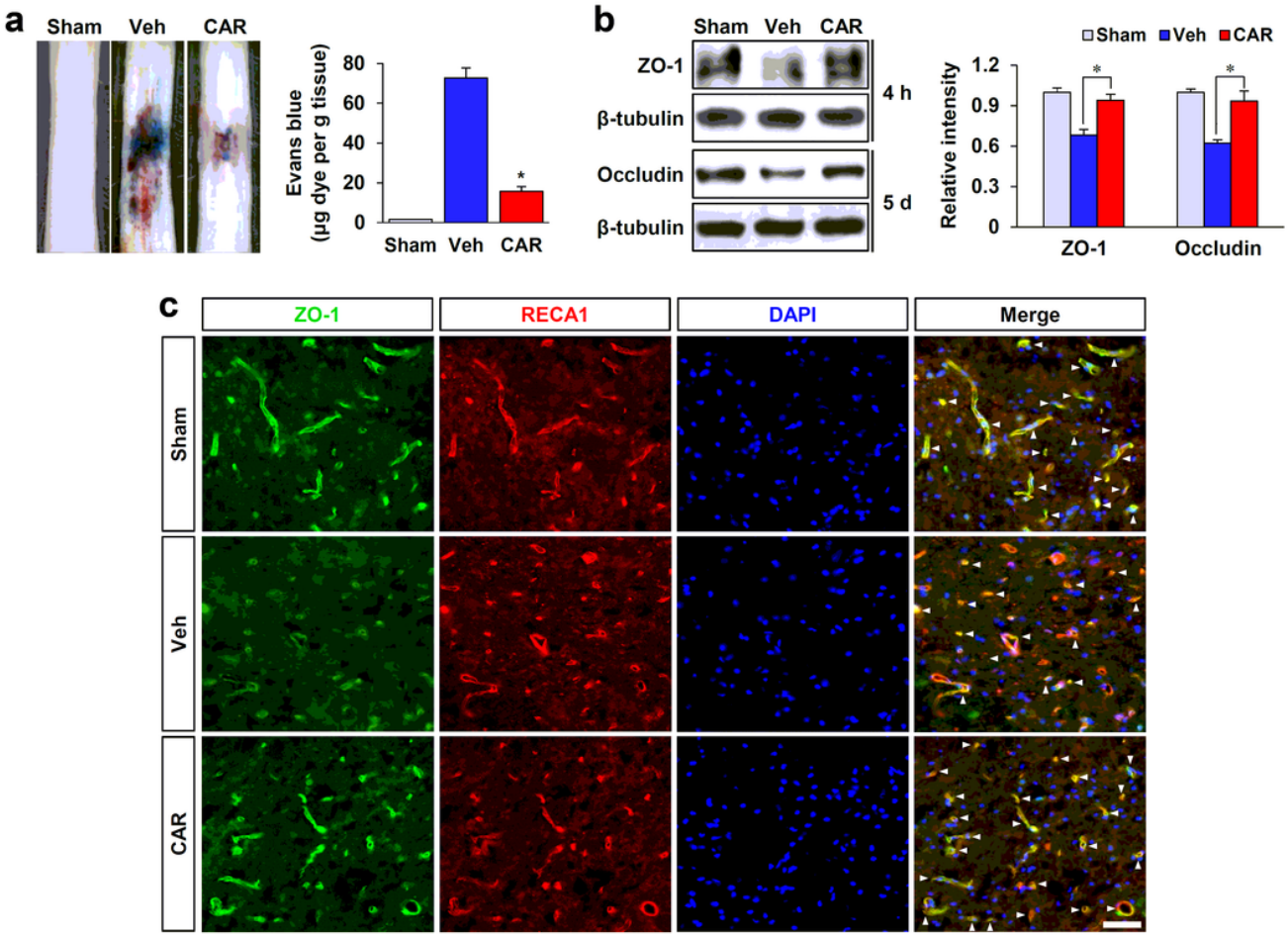

Figure 2

Carvacrol (CAR) inhibits BSCB disruption and loss of TJ proteins after injury. (A) Representative entire spinal cords demonstrating Evans blue dye extravasation into the injured spinal cord at 1 d after injury. The extravasation of Evans blue was determined with a fluorometer (excitation at 620 nm and emission at 680 nm) (n = 5). The amount of dye (μg)/tissue weight (g) was given as the value. Data represent as mean ± SEM. *p < 0.05 vs. vehicle (unpaired t-test). (B) Western blots and densitometric analysis of ZO-1 and occludin at indicated time points after injury (n = 5) (one-way ANOVA). (C) Double immunofluorescence staining showing that RECA1-positive endothelial cell expressed ZO-1 at 4 h after injury (arrow heads). Transverse spinal cord sections were selected 500 μm caudal to the lesion epicenter. Scale bar = 10 mm. Data represent mean ± SD. *p < 0.05 vs. vehicle (unpaired t-test).

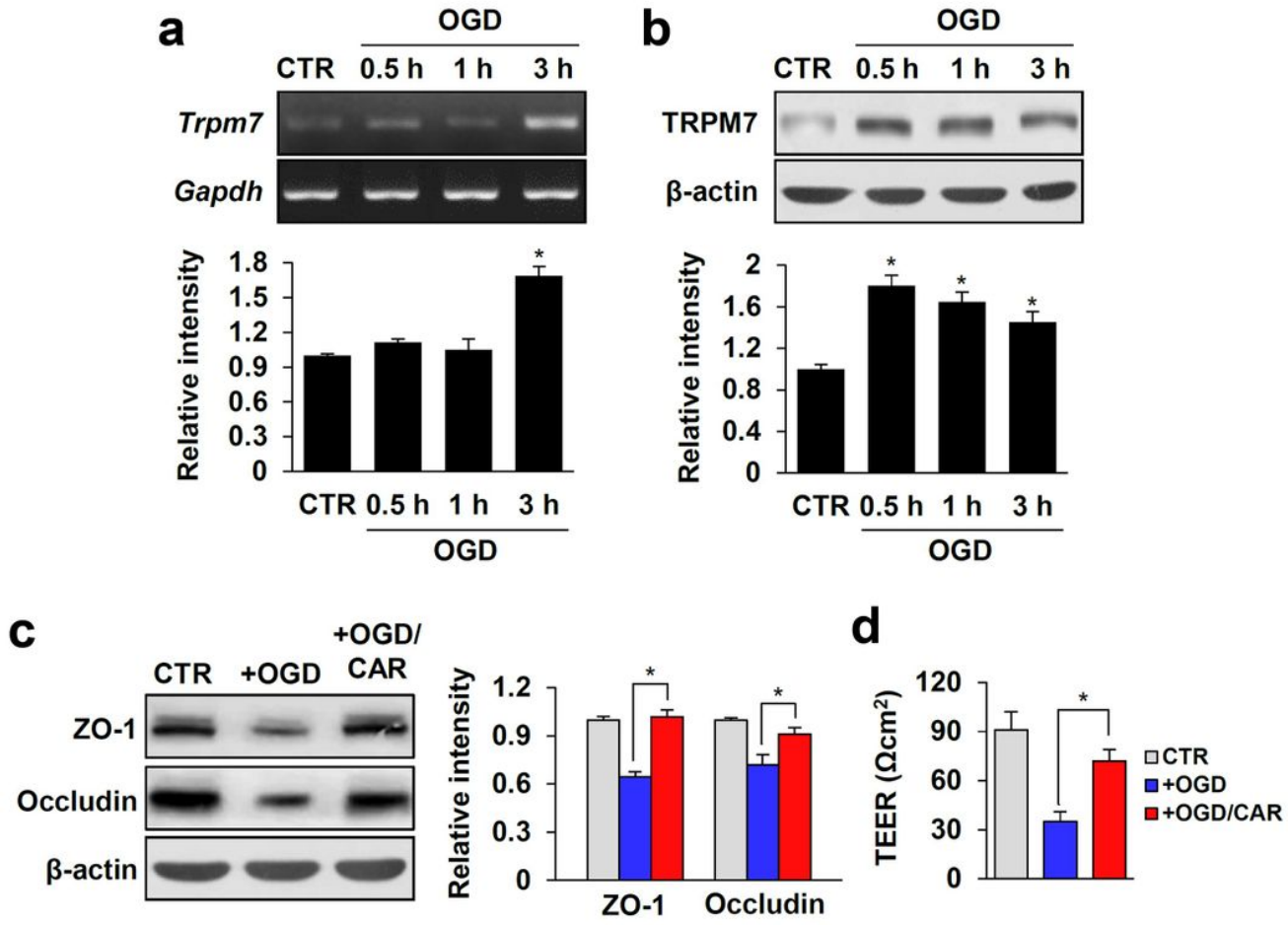

Figure 3

TRPM7 is up-regulated and contributes to the loss of TJ protein in bEnd.3 cells after OGD/reoxygenation. (A) RT-PCR and quantitative analysis for Trpm7 at 0.5 h, 1 h, and 3 h reoxygenation after OGD for 6 h. (B) Western blots and quantitative analysis for Trpm7 at 0.5 h, 1 h, and 3 h reoxygenation after OGD for 6 h. (C) Western blots and quantitative analysis for ZO-1 and occludin in bEnd.3 cell lysate treated with vehicle or CAR at 1 h reoxygenation after OGD for 6 h. (D) bEnd.3 cells were subjected to OGD/reperfusion injury after treatment with control or CAR and TEER was measured at 1 h reoxygenation after OGD as described in the Methods section. All data represent mean ± SD. *p < 0.05 vs. +OGD (one-way ANOVA).

Figure 4. CAR inhibits the infiltration of neutrophils and macrophages and the expression of the inflammatory factors after SCI

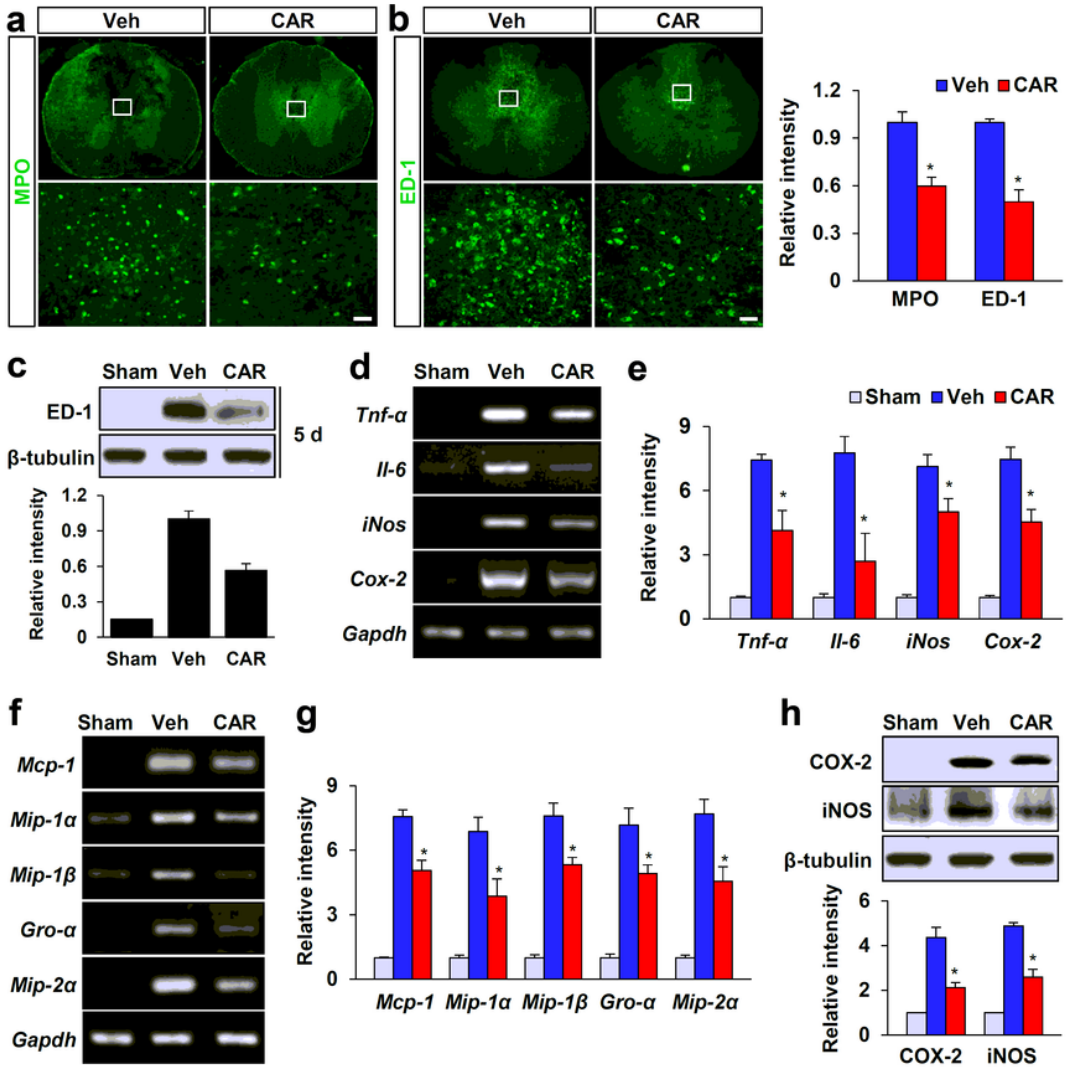

Figure 4

After SCI, CAR inhibits the infiltration of neutrophils and macrophages as well as the expression of cytokines and chemokines. Immunofluorescence images show (A) MPO-labeled neutrophils (at 1 d) and (B) ED-1-labeled macrophages (at 5 d) in the dorsal column of injured spinal cord at 1,500 and 2,000 μm rostral to lesion epicenter. Scale bars = 50 μm. (C) Relative fluorescence intensity of MPO- and ED-1-positive cells (n = 5) (unpaired t-test). (D) Western blot of ED-1 at 5 d after injury and densitometric analysis. (E) RT-PCR for Tnf-α (at 2 h), Il-6, Cox-2 and iNos (at 6 h) after injury. (F) Quantitative analysis of RT-PCR (n = 5). (G) RT-PCR after injury for MCP-1, MIP-1α, MIP-1β and MIP-2α (at 2 h), Gro-α (at 6 h) (n = 5). (H) Quantitative analysis of RT-PCR (n = 5). (I) Protein expression of iNOS and COX-2 at 1 d after SCI by Western blots and quantification analysis of Western blots (n = 5). All data represent mean ± SD. *p < 0.05 vs. vehicle (one-way ANOVA).

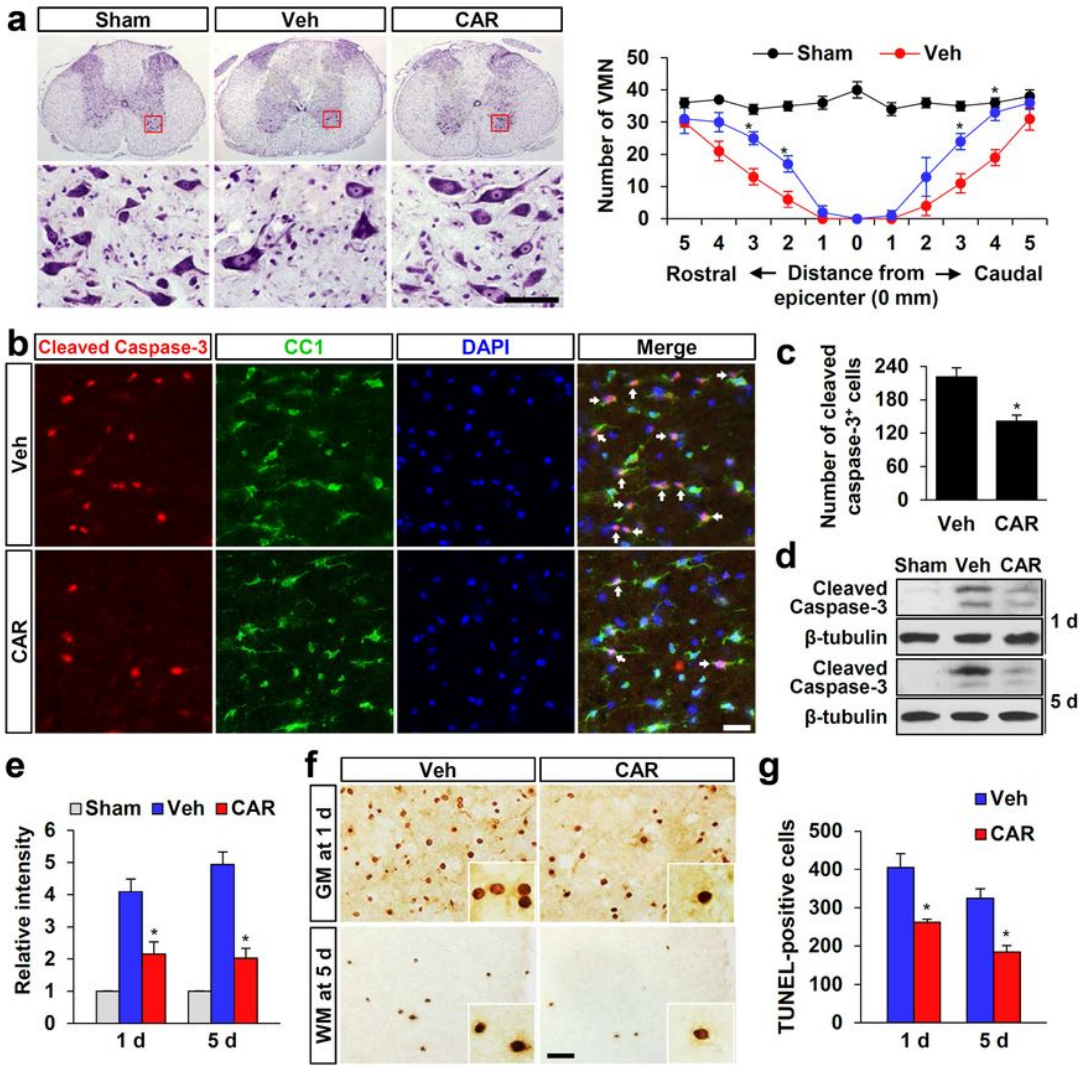

Figure 5

CAR alleviates apoptotic cell death of neurons and oligodendrocytes after SCI. (A) Representative Cresyl violet staining showing the loss of motor neurons in the ventral horn of spinal cord at 3 mm rostral from lesion site at 1 d. Scale bar = 50 μm. Spatial pattern of the number of viable motor neurons (VMN) from lesion site to 5 mm rostral and caudal region. (B) Double immunofluorescence with cleaved (active) caspase-3 (red), and CC1 (green) in the WM at 5 d after SCI. Arrows indicate CC1 and cleaved caspase-3 double positive cells. Scale bar = 30 μm. (C) Quantification of the number of cleaved caspase-3 positive cells (unpaired t-test). (D) Western blot of cleaved caspase-3 at 1 d and 5 d after injury. (E) Densitometric analysis of Western blots (n = 5). (F) Representative images of TUNEL staining at 2 mm rostral from lesion site at 1 d in the GM of spinal cord and quantitative analysis of TUNEL-positive cells. Bottom panels show representative images of TUNEL staining at 5 d after SCI in the WM (n = 5). Scale bars = 20 μm. (G) Quantitative analysis of TUNEL-positive cells in the GM at 1 d and the WM at 5 d. All data represent mean ± SD. *p < 0.05 vs. vehicle (one-way ANOVA).

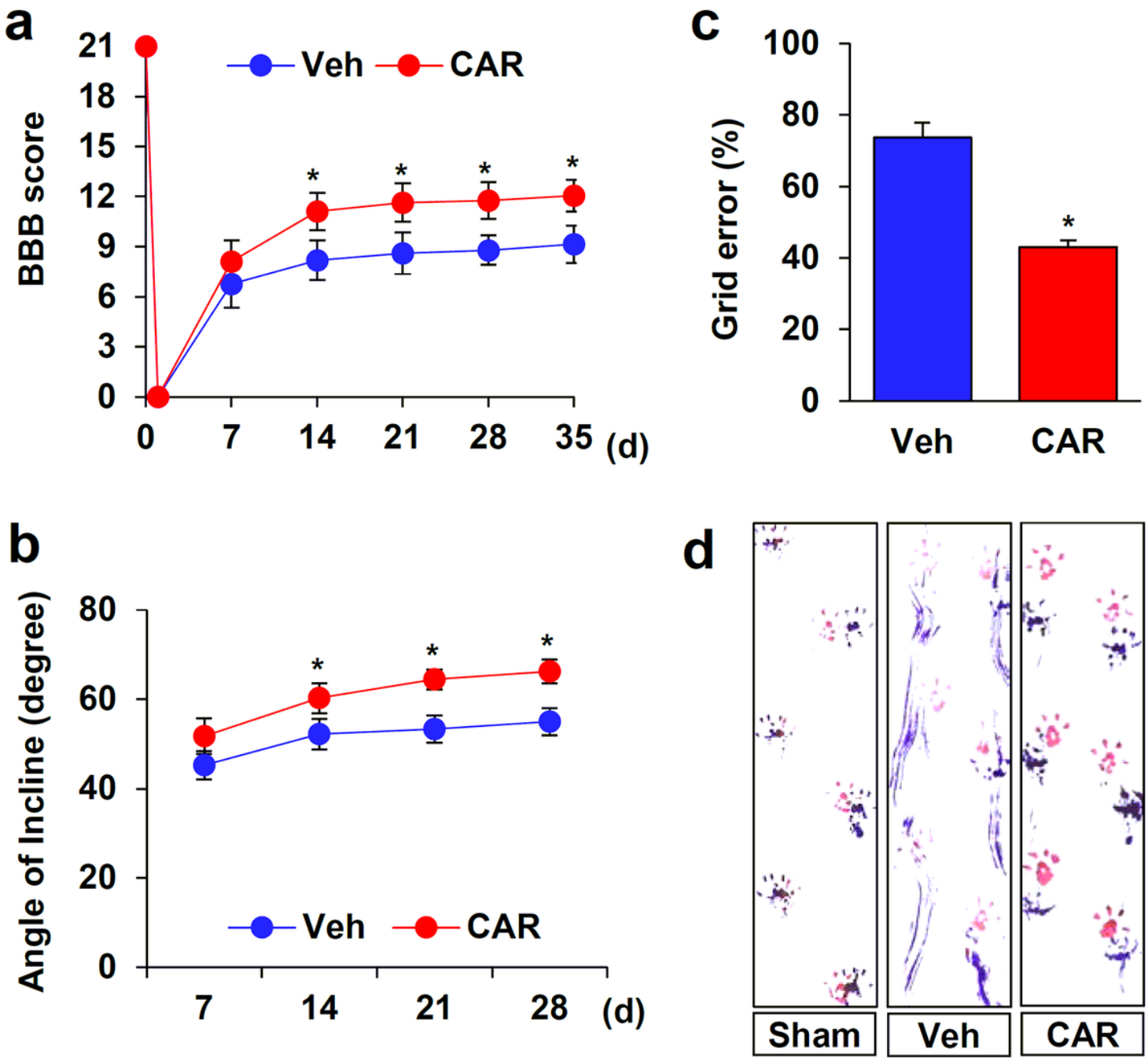

Figure 6

CAR improves functional recovery after SCI. (A) BBB open field evaluation score. (B) Test of Inclined plane. (C) Grid walk test at 35 d post-injury. (D) Foot print analysis at 35 d after SCI. All data are presented as means ± SEM (n = 10). *p < 0.05 vs. vehicle (one-way repeated measured ANOVA).

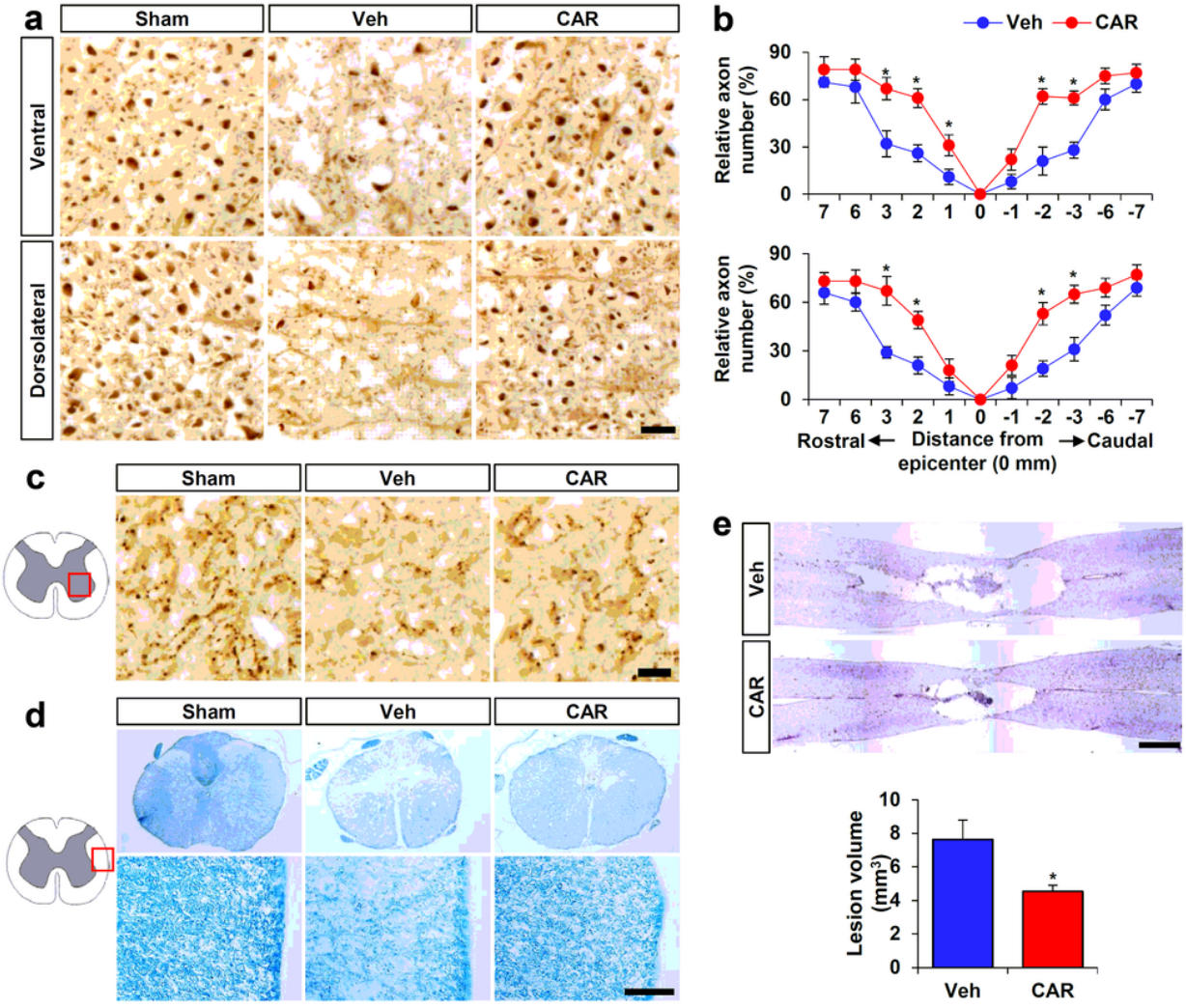

Figure 7

CAR decreases lesion volume and inhibits the loss of axon and myelin after SCI. (A) Immunohistochemical staining with NF200 showing the axon in ventral funiculi (upper) and dorsolateral funiculi (bottom) of spinal cords. 2mm rostral to the lesion site, representative photographs were chosen. (B) Counting the number of NF200- stained axons. Scale bars = 20 μm. Axons stained with NF200 were counted as described under Materials and Methods section. (C) Photographs of 5-HT-stained axons in ventral horn areas in 3 mm caudal to the lesion site. Scale bars = 30 μm. (D) Luxol fast blue staining demonstrates myelin loss in the lateral funiculus of injured spinal cord. 2mm rostral to the lesion site, representative photographs were chosen. Scale bar = 100 μm. (E) At 35 d after injury, Representative longitudinal spinal cord tissues (1.2 mm from dorsal surface) stained with Cresyl violet demonstrate cavitation of the injury area. Scale bar = 1 mm. Quantitative analysis of lesion volume (bottom). All data are presented as means ± SD (n = 5.). *p < 0.05 vs. vehicle (unpaired t-test).